Available online at www.sciencedirect.com
ScienceDirect
International Journal of Solids and Structures 45 (2008) 3674–3687
INTERNATIONAL JOURNAL OF SOLIDS AND STRUCTURES
www.elsevier.com/locate/ijsolstr

A mesoscale investigation of strain rate effect on dynamic deformation of single-crystal copper

Z.L. Liu, X.C. You, Z. Zhuang *

Department of Engineering Mechanics, School of Aerospace, Tsinghua University, Beijing 100084, China

Received 15 April 2007; received in revised form 23 July 2007
Available online 19 September 2007

Abstract

A combined finite element (FE) simulation and discrete dislocation dynamics (DD) approach has been developed in this paper to investigate the dynamic deformation of single-crystal copper at mesoscale. The DD code yields the plastic strain based on the slip of dislocations and serves as a substitute for the 3D constitutive form used in the usual FE computation, which is implemented into ABAQUS/Standard with a user-defined material subroutine. On the other hand, the FE code computes the displacement and stress field during the dynamic deformation. The loading rate effects on the yield stress and the deformation patterning of single-crystal copper are investigated. With the increasing of strain rate, the yield stress of single-crystal copper increases rapidly. A critical strain rate exists in each single-crystal copper block for the given size and dislocation sources, below which the yield stress is relatively insensitive to the strain rate. The dislocation patterning changes from non-uniform to uniform under high-strain-rate. The shear stresses in the bands are higher than that in the neighboring regions, which are formed shear bands in the crystal. The band width increases with the strain rate, which often take places where the damage occurs.

Keywords: Multi-scale; Dislocation dynamics; Flow stress; Strain rate effect; Shear band

1. Introduction

The response of materials to high-strain rates is of interest in many applications, including explosive welding, armour penetration, meteor impact, high-speed automobile and aircraft collisions, especially as the micro-electromechanical and nano-electromechanical system devices are playing an increasingly important role in modern engineering applications, such as blast-resistant design and space exploration, which involve material response on different spatial and temporal scales with various temperatures.

The response of crystal metals to high-strain-rate deformation is a complicated phenomenon, involving many physical mechanisms, such as dislocation dynamics, twinning, displacive phase transformations, grain-size, stacking fault, and solution hardening effects. Several experimental techniques have been used to

* Corresponding author. Tel./fax: +86 10 62783014.
E-mail address: zhuangz@mail.tsinghua.edu.cn (Z. Zhuang).

0020-7683/$ - see front matter © 2007 Elsevier Ltd. All rights reserved.
doi:10.1016/j.ijsolstr.2007.08.032

study the response of material to high-strain-rate, such as plate impact, SHPB, explosives, and pulsed laser loading. Recently, high intensity laser facilities coupled with X-ray diffraction techniques have been used to study the dynamic deformation process in crystalline materials (Meyers et al., 2003).

Along with the experimental techniques discussed above, computer simulation methodologies have also been used to study various dynamic deformation behaviors of material. In finite element (FE) simulation, constitutive laws are critical in the investigation of dynamic mechanical behavior of crystalline materials in application spanning from micro-scale to macro-scale, especially when materials are sensitive to strain rate. Several constitutive equations for slip have emerged, the most notable being the Zerilli and Armstrong and MTS (1987, 1990). They are based on Becker's (1925) and Seeger's (1954) concepts of dislocations overcoming obstacles through thermal activation. These constitutive models have successfully predicted that the instability strain decreases, and the yield stress increases for tantalum with increasing strain rate (Meyers et al., 2002). However, it is often impossible to get a fully physically-based constitutive model in most cases. Many fundamental issues under high-strain-rate loading, such as shear band formation and its interactions with the neighboring material, remain unclear and are worth investigation (Zhou et al., 2006).

The molecular dynamics (MD) simulations have also been performed recently to explore the mechanical properties of nano-scale materials. With the use of atomistic methods, the dislocation behavior in the plastic flow has been studied numerically by Daw and Baskes (1984), Taylor and Dodson (1990), Holian and Lomdahl (1998), Hoagland and Baskes (1998), among others. Horstemeyer et al. (2001) examined not only the spatial size but also strain rate effects on the mechanical response of single-crystal nickel by performing simple shear MD simulations using the embedded atom method (EAM). Liang and Zhou (2004) also carried out MD simulations to study the size and strain rate effects on the tensile deformation of single-crystal copper wires. Guo et al. (2007) formulated a hyper-surface to describe the combined size and strain rate effects on the plastic yield stress of fcc metals. However, it is impossible to handle not only the loading rate but also the specimen size used in the current MD simulation with existing experimental techniques. Usually, a specimen of finite size is employed in the bar or plate impact experiments to investigate the rate-dependent mechanical properties under a loading rate which is much lower than that used in the MD simulation so far.

As can be seen from the opening literature, much research works have been conducted to investigate the rate-dependence of material properties at atomic-scale and macro-scale, respectively. However, little has been done in understanding loading rate effects on the mesoscale, since many important failure forms, such as shear instability, fracture, take place on the mesoscale (Needleman, 1999).

Over the last decade, 3D dislocation dynamics (DD) has emerged as an excellent numerical tool for crystal plasticity simulation on the mesoscale (Devincre and Kubin, 1997; Fivel, 1998), by which the simulated size can be of tens of several microns, exceeding by an order of magnitude the capabilities of MD simulations. Moreover, DD simulation can be used directly as material constitutive functions for continuum simulations (Lemarchand and Devincre, 2001), so it has the potential to bridge atomistic simulation and macroscopic simulation (Tadmor et al., 2000).

In this study, a combined FEM/discrete dislocation dynamics (DD) approach is firstly developed, and this model in 3D is implemented in a user-defined subroutine ABAQUS/Standard code in Section 2. The computational model is described in Section 3. In Section 4, the loading rate effects on the yield stress and the deformation patterning of single-crystal copper are investigated. Conclusions are given in the last section.

2. Coupling dislocation dynamics plasticity with FEM

The multi-scale model combines discrete dislocation dynamics and continuum finite element. In our method, a discrete dislocation dynamics code is substituted for the constitutive form traditionally used in finite element calculation. A 3D DD code solves the dynamic and local reactions of discrete dislocation lines and computes the plastic strain generated by dislocation glide. On the other hand, a FE code computes the stress and displacement field, providing a solution to the boundary value problem by making use of the plastic strain field developed by the DD simulation.

In the present work, we present a computational model coupling 3D discrete dislocation dynamics code (microMegas) with FEM software ABAQUS. More details of microMegas can be found in a series of papers by Devincre and Kubin (1997, 2001, 2006). To combine with FEM code and deal with the high velocity of

dislocations in dynamic deformation, some modifications have been made. Here, we provide some descriptions.

2.1. Resolution of the dislocation dynamics

Dislocation dynamics (DD) is a mesoscale approach that simulates the dynamic behavior of a large number of curved dislocations on a finite length. Simulations based on discrete dislocations are mechanism-based, allowing the effects of dislocation motion and dislocation interactions to be analyzed.

In 3D DD, dislocations are discretized into segments of mixed character. The self-stress field of a straight dislocation segment in an infinite solid serves as the basis of DD code. Since the stress field of the dislocation varies with the inverse of distance from the dislocation core, dislocations interact among themselves over long distances. As the dislocation moves, it has to overcome internal drag, and local barriers such as Peierls stress. The dislocation may encounter local obstacles such as defect clusters and vacancies, which interact with the dislocation at short ranges and affect its local dynamics. The Peach-Koehler force acting on each dislocation is calculated at the center of each dislocation segment, and the effective force on segment i is given by:

$$\mathbf{f}_i = (\boldsymbol{\sigma} \cdot \mathbf{b}_i) \times \xi_i + \mathbf{f}_{\text{self}} \tag{1}$$

where $\mathbf{b}_i$ is Burgers vector of segment i,and ξ_i is the line sense unit vector describing its direction, $\mathbf{f}_{\text{self}}$ is the self force caused by the nearest neighbor segments, $\boldsymbol{\sigma}_i$ is the total stress tensor estimated at the center of segment i and it can be decomposed into:

$$\boldsymbol{\sigma}_i = \boldsymbol{\sigma}^{\text{applied}} + \boldsymbol{\sigma}^{\text{interaction}} + \boldsymbol{\sigma}^{\text{other}} \tag{2}$$

where $\boldsymbol{\sigma}^{\text{applied}}$ is the externally applied stress, which is computed by FEM in our multi-scale model, $\boldsymbol{\sigma}^{\text{interaction}}$ is the contribution of the stress field of the other dislocation segments, $\boldsymbol{\sigma}^{\text{other}}$ arises from the interaction of dislocations with other defects or free surfaces, which can also be computed by FEM.

The velocity, v, of a dislocation segment is governed by a first order differential equation consisting of an inertia term, a drag term and a driving force such as:

$$m^*(v)\dot{v} + Bv = F = \tau b \tag{3}$$

where μ^* is the effective mass in dislocation segment. B is viscous drag coefficient, b is the magnitude of Burgers vector, τ is the resolved effective stress. Because the initial acceleration of dislocation is very high, the dislocations can reach a stable velocity in a very short time, and the corresponding moving distance is so small, less than 1 nm, that it can be neglected. Thus we assume that dislocation immediately reaches a stable velocity (Gillis and Kratochvil, 1970; Meyers, 1994) such as:

$$Bv = \tau b \tag{4}$$

Gillis et al. (1969) suggested that Eq. (4) might be extended to higher velocities by replacing B with:

$$B = \frac{B_0}{1 - v^2/v_s^2} \tag{5}$$

where B_0 is static viscous drag coefficient, v_s is the speed of shear wave. Substituting Eq. (5) into Eq. (4), we can get the stable velocity.

$$v = \frac{v_s}{2}\left(\sqrt{\left(\frac{v_s B_0}{\tau b}\right)^2 + 4} - \left(\frac{v_s B_0}{\tau b}\right)\right) \tag{6}$$

with $v_s = 2.92 \times 10^3$, $b = 2.55 \times 10^{10}$, $B_0 = 5 \times 10^{-5}$, the velocity of dislocation versus resolved shear stress is plotted in Fig. 1. As the resolved shear stress increases, the velocity approaches the speed of shear wave.

Then the evolving dislocation structure can be simulated, such as bowing out, expansion/shrinkage of loops and pile-up.

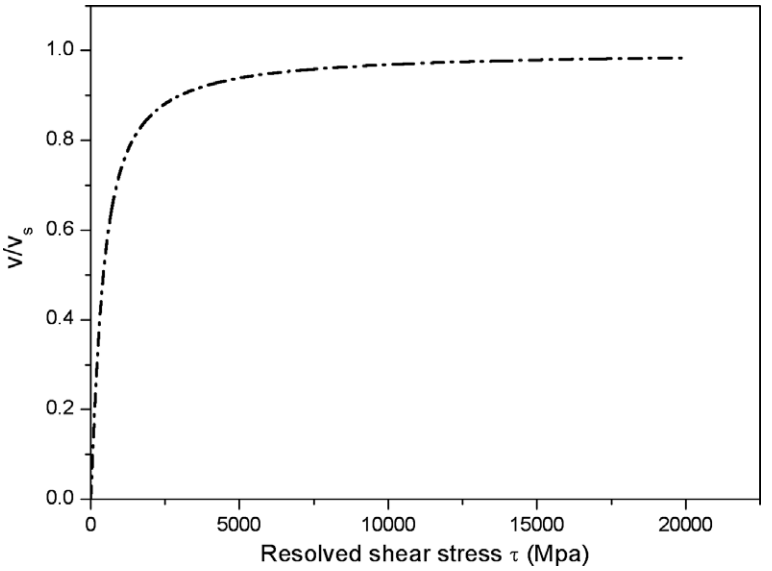

Fig. 1. Variation of the dislocation velocity (normalized by the speed of shear wave) with resolved shear stress.

2.2. Elastic-viscoplastic continuum mechanics

The kinematics and constitutive relationships of mesoplasticity that follows those of Peirce et al. (1982) are used in this paper. The velocity gradient can be expressed as:

$$\mathbf{L} = \mathbf{D} + \mathbf{\Omega} \tag{7}$$

where $\mathbf{D}$ is the symmetric part of the rate of deformation and $\mathbf{\Omega}$ is the skew symmetric spin tensor. $\mathbf{D}$ and $\mathbf{\Omega}$ are additively decomposed into elastic parts ($\mathbf{D}^{e}$ and $\mathbf{\Omega}^{e}$) and plastic parts ($\mathbf{D}^{p}$ and $\mathbf{\Omega}^{p}$), respectively, as follows:

$$\mathbf{D} = \mathbf{D}^{e} + \mathbf{D}^{p} \tag{8}$$

$$\mathbf{\Omega} = \mathbf{\Omega}^{e} + \mathbf{\Omega}^{p} \tag{9}$$

Assuming that the crystal elasticity is unaffected by slip, the elastic constitutive equation is given by:

$$\overset{\nabla}{\boldsymbol{\sigma}}{}^{e} = \mathbf{C}^{e} : \mathbf{D}^{e} \tag{10}$$

Where $\mathbf{C}^{e}$ is the tensor of elastic moduli, $\overset{\nabla}{\boldsymbol{\sigma}}{}^{e}$ is the Jaumann rate of Cauchy stress $\boldsymbol{\sigma}$, which is the co-rotational stress rate in terms of the coordinate system that rotates with the lattice. $\overset{\nabla}{\boldsymbol{\sigma}}{}^{e}$ is determined by

$$\overset{\nabla}{\boldsymbol{\sigma}}{}^{e} = \overset{\nabla}{\boldsymbol{\sigma}} + \mathbf{\Omega}^{p} \cdot \boldsymbol{\sigma} - \boldsymbol{\sigma} \cdot \mathbf{\Omega}^{p} \tag{11}$$

Where $\overset{\nabla}{\boldsymbol{\sigma}}$ is the co-rotational stress rate on the coordinate system that rotates with the material. In small strain

$$\mathbf{\Omega}^{p} = 0, \quad \overset{\nabla}{\boldsymbol{\sigma}} = \overset{\nabla}{\boldsymbol{\sigma}}{}^{e} = \mathbf{C}^{e} : \mathbf{D}^{e} \tag{12}$$

2.3. Coupling framework

Van der Giessent and Needleman (1995) combined 2D dislocation dynamics with finite element to solve the boundary value problem of finite crystal, making use of the superposition principle. The solution of the boundary value problem is obtained as the sum of two contributions. The first represents the solution for dislocations in an unbounded continuum and the other is the complementary elastic solution needed to satisfy equilibrium at external and internal boundary. The last contribution is computed by a FE code.

Based on superposition principle, the boundary value problem of finite crystal can be cast into a standard FE framework, and has the following general form:

$$\mathbf{Ma} + \mathbf{f}^{\text{int}} = \mathbf{f}^{\text{ext}} \tag{13}$$

where

$$\mathbf{f}^{\text{ext}} = \mathbf{f}^{\text{a}} + \mathbf{f}^{\text{im}} + \mathbf{f}^{\text{dis}} \tag{14}$$

where, $\mathbf{f}^{\text{int}} = \int_v \mathbf{B}^{\text{T}}\boldsymbol{\sigma}\,\mathrm{d}v$ is internal force vector, $\boldsymbol{\sigma}$ is the total stress tensor, and can be computed by Eq. (11), $\mathbf{f}^{\text{a}} = \int_S \mathbf{N}^{\text{T}}\mathbf{t}^{\text{a}}\,\mathrm{d}s$ is applied force vector, $\mathbf{t}^{\text{a}}$ is traction applied on the stress boundary, $\mathbf{f}^{\text{im}} = \int_S \mathbf{N}^{\text{T}}\mathbf{t}^{\text{im}}\,\mathrm{d}s$ is the image force vector, $\mathbf{t}^{\text{im}}$ is traction arising from the interaction of dislocations with free surface, the image field can be solved by Boussinesq-Cerruti formalism accurately or Lothe-force approximation (Liu and Schwarz, 2005), $\mathbf{f}^{\text{dis}} = \int_V \mathbf{B}^{\text{T}}\boldsymbol{\sigma}^{\text{dis}}\,\mathrm{d}V$ is a "body force" (Zbib and Diaz de la Rubia, 2002) in the crystal, $\boldsymbol{\sigma}^{\text{dis}}$ is the stress tensor of the dislocations in an infinite crystal. $\mathbf{N}$ is shape function vector, and $\mathbf{B} = \text{grad}[\mathbf{N}]$.

The key of this method is connecting the observed macroscopic parameters (used in continuum models), such as stress and strain at material points, to the elementary shears produced by a constitutive relationship with dislocations. A direct linkage to continuum codes will be too inefficient to make computation practical. As FE calculations typically involve large number of material points, each with its own stress–strain trajectory, running a statistically representative DD simulation for each material point simultaneously will remain prohibitively expensive for years to come (Bulatov, 2002). So within the continuum framework, we choose a representative volume element (RVE), in which the deformation field is assumed to be homogeneous (Zbib and Diaz de la Rubia, 2002). The dislocation dynamics model is presumably capable of describing the heterogeneous nature of the deformation field. With a proper homogenization theory, or field averaging, one can couple the discrete dislocation dynamics model with continuum mechanics.

The macroscopic plastic strain $\mathbf{D}^{\text{p}}$ and plastic spin $\boldsymbol{\Omega}^{\text{p}}$ are evaluated at the Gauss points, and can be related to the motion of each dislocation segment:

$$\begin{aligned} &\mathbf{D}^{\text{p}} = \frac{\Delta\gamma}{2}(\mathbf{n_i}\otimes\mathbf{b_i} + \mathbf{b_i}\otimes\mathbf{n_i}), \quad \boldsymbol{\Omega}^{\text{p}} = \frac{\Delta\gamma}{2}(\mathbf{n_i}\otimes\mathbf{b_i} - \mathbf{b_i}\otimes\mathbf{n_i}), \\ &\Delta\gamma = \rho b v = \sum_{i=1}^{N}\frac{l_i b v_{gi}}{V} \end{aligned} \tag{15}$$

where V is the volume of representative volume element (RVE) that includes the integration point, N is the number of segments that slip through the element in Δt (the time step in FE simulation), l_i is the length of segments i, v_{gi} is the dislocation glide velocity, $\mathbf{n_i}$ is the unit normal to the slip plane, $\mathbf{b_i}$ is the burgers vector.

Eqs. (11), (15) and (14) can be implemented in ABAQUS/Standard by a user-defined material subroutine UMAT and a user-defined load DLOAD, respectively.

The Eq. (13) can be solved with Newmark β integration method in ABAQUS, and then the stress and displacement fields are obtained in the finite single-crystal. Once the stress field in the crystal is known, the Peach-Koehler force can be estimated on all the dislocation segments. Anew plastic step is performed by the DD code repeatedly.

3. Model description

We consider an isotropic copper single-crystal with the following properties (relevant to both the continuum model and DD model), shear modulus $\mu = 42$ GPa, Poisson's ratio $v = 0.347$, density $\rho = 8900$ kg/m^3, magnitude of Burgers vector $b = 2.5525$ Å, and static viscous drag coefficient $B_0 = 5.5 \times 10^{-5}$ Pa s^{-1}. Temperature is 300 K.

As illustrated in Fig. 2, the simulation setup consists of a block with dimensions $5 \times 5 \times 10$ μm, which is divided into a finite element mesh using eight-node brick elements. The bottom surface of the sample is fixed, and the upper surface is moved at controlled rate so that the strain rate, ranging from 10^2 to 10^5 s^{-1}, is made constant (the displacement of the upper surface increases in time). All other surfaces are assumed to be free,

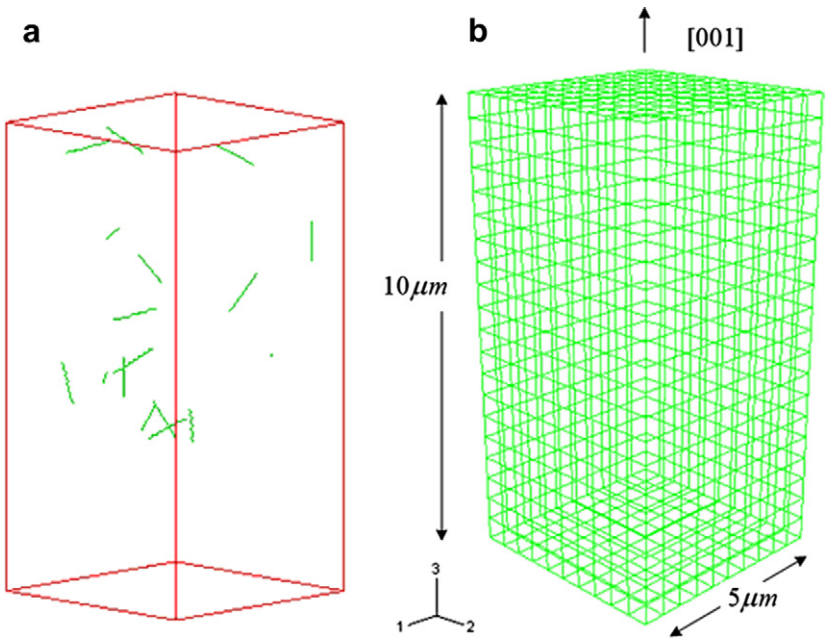

Fig. 2. (a) The initial dislocation line distribution in the single-crystal copper; (b) dimension of simulation cell and the FE mesh.

where, the tractions, resulting from the interaction of dislocations with free surfaces, are computed at four integration points.

Fig. 2(a) shows the initial state of dislocations in the simulation block. The mobile dislocation density is zero. Sixteen dislocation lines pinned at two ends are distributed randomly in the crystal, and the length of each dislocation line is 1 μm. They are located in the four different slip systems,$(111)[10\bar{1}]$, $(1\bar{1}1)[\bar{1}01]$, $(11\bar{1})[110]$, $(\bar{1}11)[011]$, and Schmid factors are 0.408, 0.408, 0.408, 0, respectively. Each slip system possesses four dislocation sources, and the dislocation density is about $6.4\times10^{10}\ \mathrm{m}^{-2}$.

Various finite element meshes were examined ranging from very coarse $5\times5\times10$ to very fine $20\times20\times40$. Here the results with $10\times10\times20$ are presented, which is fine enough to reflect the deformation patterning of dislocation structure. The time step of DD computation is chosen from 10^{-9} to 10^{-11} with the increasing of strain rate, and is one order lower than that of FE simulation.

4. Simulation results and discussions

The plastic flow of the metal single-crystal is determined by many factors, including crystal orientation, temperature, applied strain rate, specimen size, deformation path, and the microstructure of material. The focus of the present work is on the microstructure and strain rate effects.

4.1. Strain rate effect on yield stress

The stress–strain curves are computed by elements average values. Four different strain rates are plotted in Fig. 3, from which we can see, the curves can be distinctly divided into three segments, including an elastic part, a strain hardening part, and a strain softening part. The initial transient peak in Fig. 3 is caused by an artifact related by the initial configuration: initially the mobile dislocation density which is too small to achieve the imposed strain rate as the pinned segments sources cannot be activated. In cases where the initial configuration has a higher density of dislocation which can accommodate more rapidly the strain rate, the transient peak is absent. The slight oscillations and a stress drop-off in Fig. 3 are a result of the heterogeneous nature of the activation and progression of dislocations.

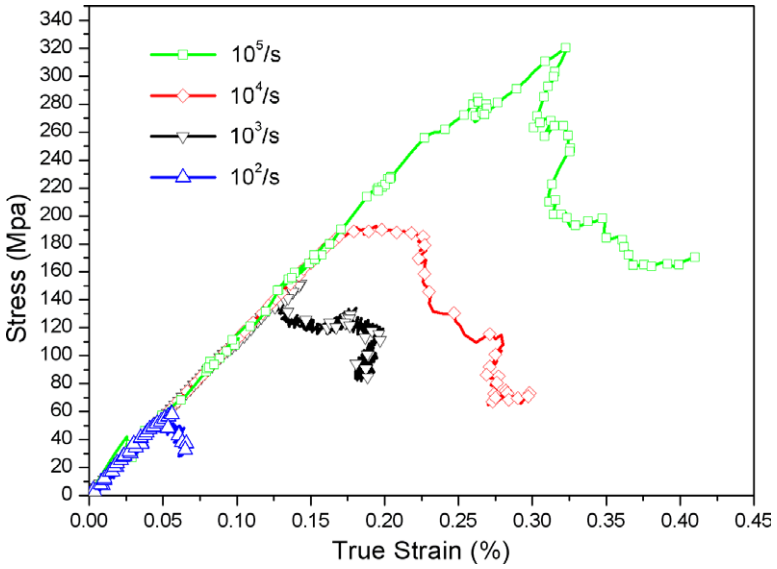

Fig. 3. Stress–strain curves of single-crystal copper block of $5 \times 5 \times 10$ (μm^3) at different strain rates.

The transition point between the elastic part and the strain hardening part can be regarded as the stress yield point. From Fig. 3, it is clear that the yield stress increases with the increasing strain rate. This phenomenon was discovered by Edington (1969) in the uniaxial compression tests of copper specimen the size of several millimeters, and by Horstemeyer et al. (2001) in the simple shear atomistic simulations of single-crystal nickel, and by Guo and Zhuang (2007) in the simple shear MD simulations of single-crystal copper, as shown in Fig. 4.

To understand the rate effect of single-crystal copper on the mesoscale, a quantitative analysis is carried out based on our multi-scale simulation results. The flow stress τ of crystal material is composed of two components:

$$\tau = \tau_\mu + \tau^* \tag{16}$$

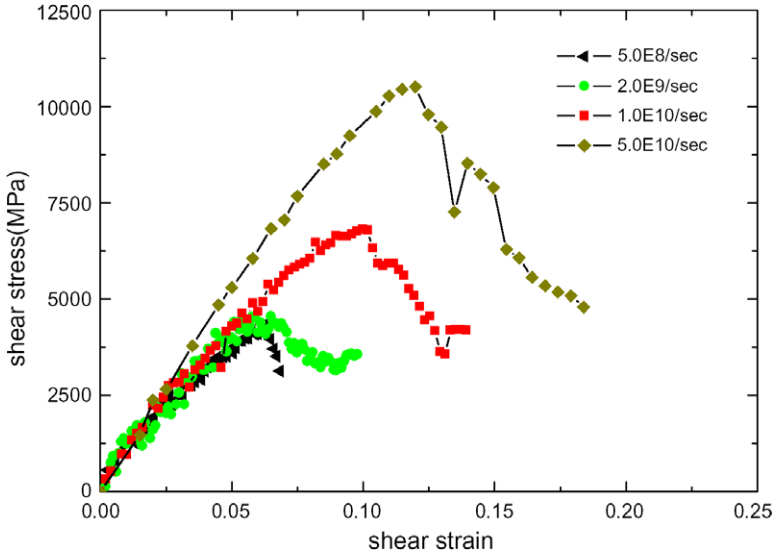

Fig. 4. Shear stress–strain curves of single-crystal copper block of $32.35 \times 10.98 \times 2.40$ (nm^3) at different strain rates (Guo et al., 2007).

$\tau^*$is the effective stress on the dislocation, which governs the thermally activated motion of dislocations through localized obstacles like Peierls barriers (Hirth and Lothe, 1982), τ_μ is the athermal stress on the dislocation, which stems from the long range elastic interaction with all the other dislocations and the short range dislocation–dislocation interaction.

At normal temperature and strain rate, for FCC single-crystal, the thermally activated resistance is very small, which are mainly Peierls barriers, just about 0.5 MPa for single-crystal copper. It can be easily overcome, so the contribution of τ^* to flow stress can be neglected. In this case, the flow stress τ is mainly determined by the athermal τ_μ. In other words, the short-range reactions between dislocations are responsible for most of the flow stress. In our simulation, it is mainly decided by the critical stress, τ_{FR}, for the operation of a Frank-Read source, and the non-local contribution typically is of the order of 0.1–0.15 τ_{FR} for segment length in the micrometer range (Devincre and Condat, 1992), the influence of surface correction is neglected. The critical resolved stress for pinned dislocation line can be expressed as:

$$\tau_{FR} = 2\alpha\frac{\Gamma}{bl} \approx 2\alpha\frac{\mu b}{l}, \quad \tau_\mu \approx \tau = 1.15\tau_{FR} \tag{17}$$

where $\Gamma \approx \mu b^2$ is the line tension of the dislocation, μ is the shear modulus, b is the magnitude of the Burgers vector, α is a parameter that quantifies the strength of the obstacle, for FR source, $\alpha \approx 1$, $l = 1$ μm, is the length of dislocation line. We get,

$$\tau_\mu = 5.88 \times 10^{-4}\mu = 24.73 \text{ MPa} \tag{18}$$

As can be seen from Eq. (17), when the average length of the dislocation line, l, is governed by one specimen dimension, a size effect arises.

Once the critical resolved stress is obtained, the initially pinned dislocation lines are activated and begin to bow out (Fig. 5). The yielding begins when there is a balance between the dislocation-induced plastic strain increment and the boundary-imposed strain rate, so when the yield stress is achieved, more and more Frank-Read sources become operative to accommodate the high-strain-rate deformation with increasing strain rate, as shown in Fig. 6.

Assuming the flow stress τ is the maximum shear stress, we can estimate the static yield stress $\sigma_s = 2\tau = 49.46$ Mpa $= 0.001176\mu$ for our present simulation, which accords well with the value obtained under the strain rate 100 s^{-1}, as shown in Fig. 3.

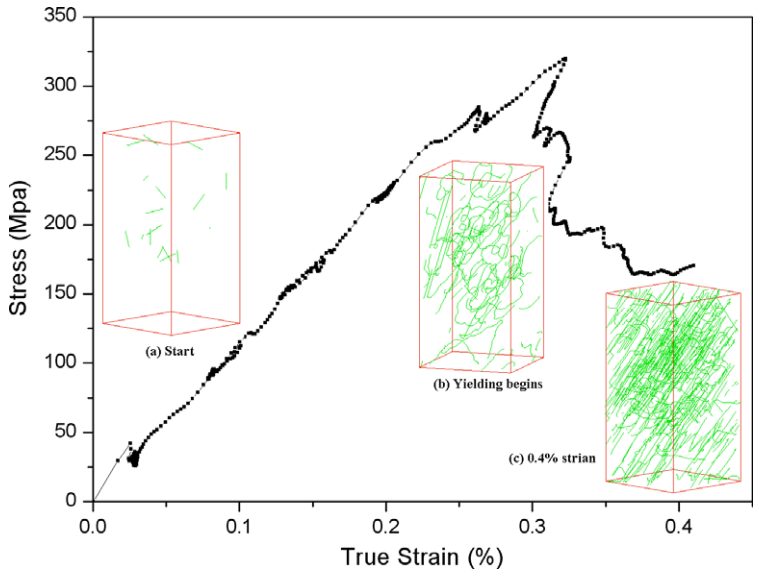

Fig. 5. Stress–strain curve under strain rate 10^5 s^{-1}, and the corresponding dislocation states illustrating activation and motion of dislocation lines at different strain.

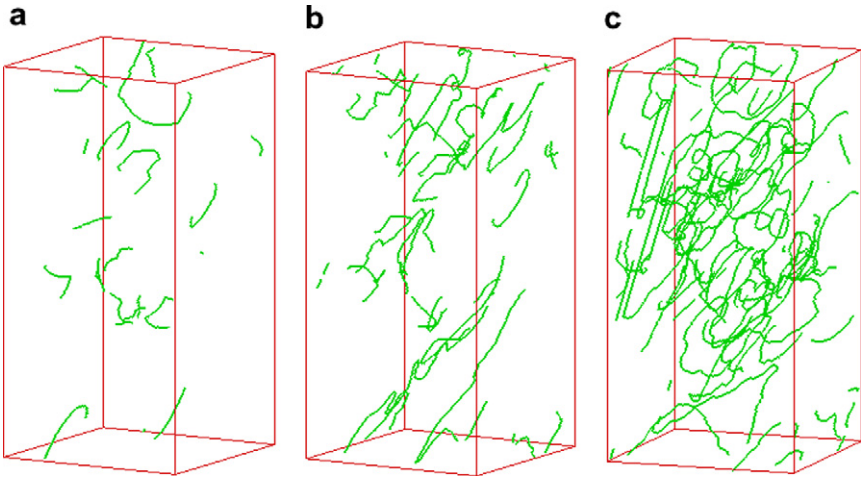

Fig. 6. The dislocation microstructure at the yield point under strain rate (a) $10^3\ s^{-1}$, (b) $10^4\ s^{-1}$, (c) $10^5\ s^{-1}$. More and more Frank-Read sources are operating to accommodate the high-strain-rate deformation with increasing strain rate when yielding occurs.

When the strain rate is high, according to the Orowan's law, which relates the total strain rate to the dislocation flux:

$$\dot{\gamma} = \rho b v \tag{19}$$

where, v is the average velocity of dislocations. Increasing the strain rate is equivalent to increasing the average velocity according to Eq. (19). We have the expression of effective stress τ^* and the velocity for viscous type used in pure FCC metals:

$$\tau^* = \frac{Bv}{b} = \frac{B\dot{\gamma}}{b^2\rho}, \quad B = \frac{B_0}{1 - v^2/v_s^2} \tag{20}$$

The coefficient B accounts for electron and phonon drag, it also impedes the motion of dislocations with the increasing strain rate. Assuming that the dislocation density ρ is not significantly modified, a high-stress level is necessary to achieve the imposed velocity, and it will become larger than what is needed for crossing forest obstacles τ_μ, with the increasing strain rate. In other words, increasing the strain rate is equivalent to increasing the thermally activated glide resistance of dislocations. The same effect can be obtained by decreasing the temperature. They all make the movement of dislocation more difficult.

So according to Eq. (20), when $\dot{\gamma}$ is larger than some critical value, $\dot{\gamma}_c$, τ^* will dominate the value of flow stress, then the yield stress will be strongly strain rate sensitive. According to $\tau^* > \tau_\mu$, $\dot{\gamma}_c$ is controlled by the value of $\frac{\alpha\mu b^3}{B}\left(\frac{\rho}{l}\right)$, which is decided by the dislocation density, the size of the dislocation source (the distance between the two pinned ends of the source), the size of the specimen, or simply the average size of the dislocation mean free path, and the strength of the obstacles. In our simulation, the crystal strain rate is 10^2–$10^3\ s^{-1}$. The yield stress normalized by the shear modulus (NRYS) is plotted as a function of strain rate in Fig. 7, which yields the following linear relation with a correlation coefficient $r^2 = 0.99$:

$$\frac{\sigma_s}{\mu} = 0.00162 \cdot \log\dot{\varepsilon} - 0.00186 \tag{21}$$

Above the critical strain rate, the yield stress normalized by the shear modulus has a linear relationship with $\log\dot{\varepsilon}$, and a similar conclusion was drawn through experiments in tantalum (Chen et al., 1999) and copper (Follansbee and Gray, 1991).

Yield stress is also very sensitive to the applied loading rate under the high-strain-rate at the atomic-scale (Guo and Zhuang, 2007), where the effects of dislocation inertia and phonon drag are important. A higher strain rate requires higher acceleration and velocity of the dislocations nucleated in the specimen to accommodate the quick deformation. Therefore, a higher yield stress is required to overcome the inertial force and

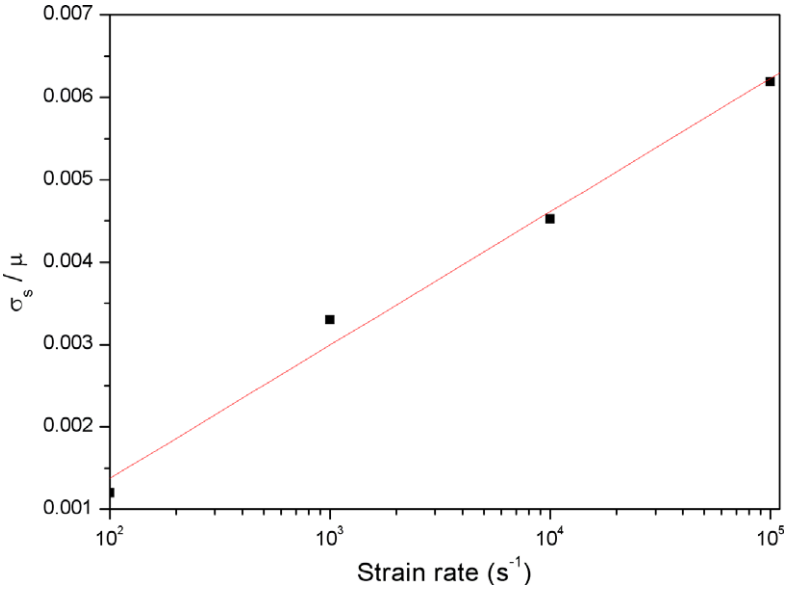

Fig. 7. Normalized resolved yield stress versus four different strain rates. The linear regression line has a correlation coefficient r^2=0.99.

phonon drag force acting on the dislocations for the larger specimen under high-strain-rate. On the mesoscale, the initial dislocation density, the average size of the dislocation mean free path, and the strength of the barriers of dislocation are also affecting the yield stress considerably under the high-strain-rate besides the specimen size.

4.2. Strain rate effect on the deformation patterning

The dislocation patterning is also determined by the ratio of τ_μ/τ^*: when τ_μ dominates the flow stress, the dislocation–dislocation interaction is strong, and the multi-body interaction effect is evident. One can observe dislocation patterning in crystal; with τ^* playing a dominant role, dislocation–dislocation interaction is comparatively weak, each dislocation moves as if it is alone in the crystal, the dislocation microstructure exhibits no patterning, as can be seen in Fig. 8(a)–(c), respectively. Dislocation microstructures change from non-uniform to uniform.

In single-crystal copper, there are 12 different slip systems, which can contribute to the deformation process. The slip systems are listed in Table 1 as combinations of the slip planes and slip direction. The contribution of each slip system to the plastic deformation at different strain rates is investigated by plotting the dislocation density distribution of each slip system, as shown in Fig. 9. The dislocation tends to become localized in one slip system, $(1\bar{1}1)[\bar{1}01]$, and in the areas of the simulated crystal where dislocation multiplication is the most active (Fig. 8), the number of initial dislocation sources in each slip system is the same. This may be attributed to the interaction process between the dislocations in the different systems.

Under high-strain-rate, the presence of active dislocation sources in rapidly deforming crystalline material can serve as the focus of localized plastic flow and associated energy concentrations that in turn determine the mechanical response of material. Most of these localized regions manifest themselves often in the form of shear band (Wright, 2002). In our simulation, deformation band can be observed clearly, as shown in Fig. 8(a)–(c). From the simulation results, it can be observed that the deformation is mostly localized in the bands along the most active slip plane $(1\bar{1}1)$, and with the strain rate increasing, the width of the band is also increasing from 2 μm to several tens of micrometer, which is restricted by the size of simulated crystal. In the experiments of bulk crystal material, the width of shear band is often hundreds of micrometers. In our simulation, it can be seen that very few dislocation sources are responsible for creating the dislocations that form the shear band. Under extremely high-strain-rate, such as shock loading (up to 10^{10} s^{-1}), as the classical

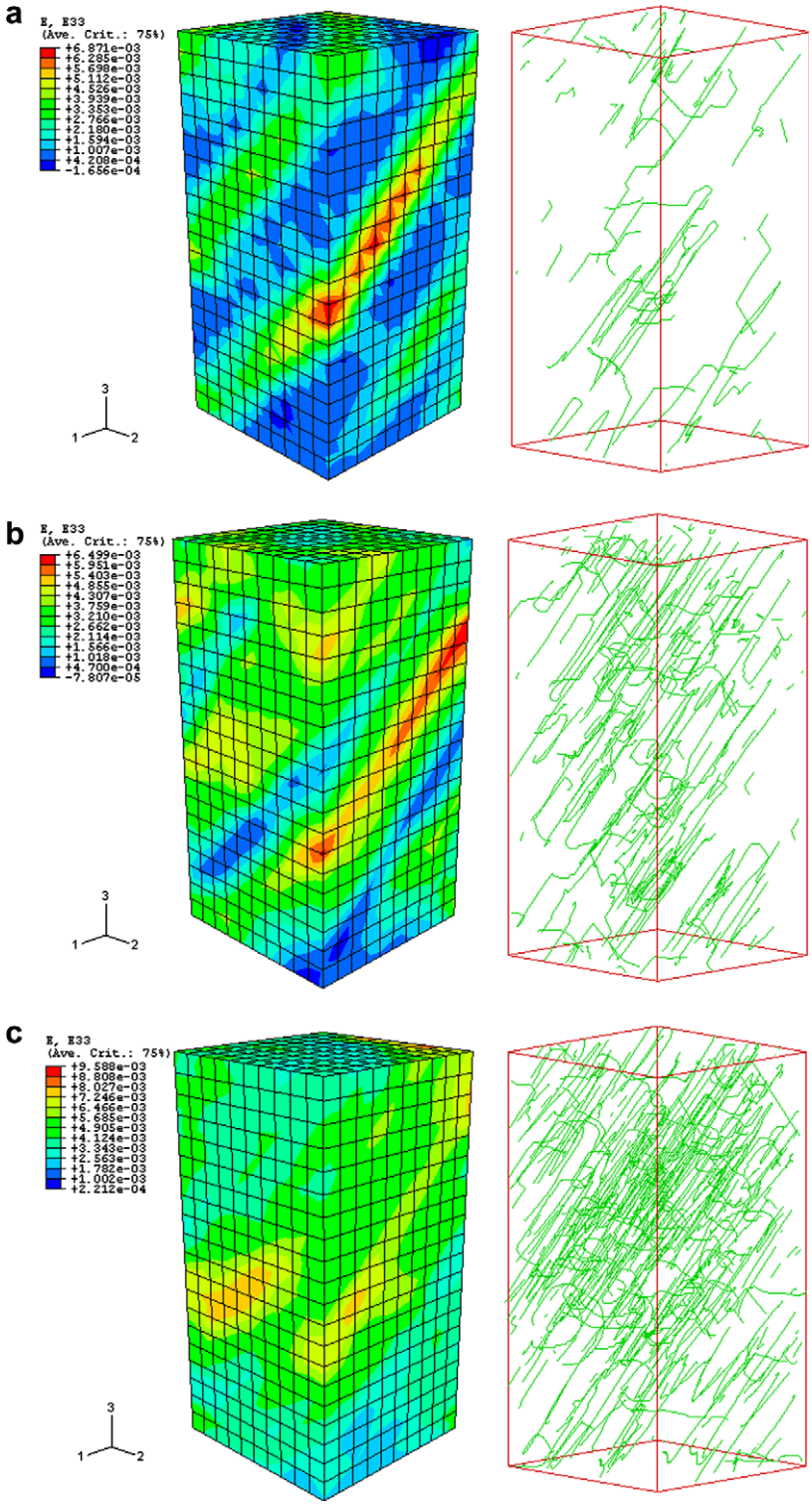

Fig. 8. Distribution of strain ε_{33} in the crystal and corresponding dislocation microstructure after yield under strain rate (a) $10^3\ s^{-1}$, (b) $10^4\ s^{-1}$, (c) $10^5\ s^{-1}$. The deformation is mostly localized in the bands along the most active slip plane $(1\bar{1}1)$, and with the strain rate increasing, the width of the band is also increasing.

Table 1
Slip systems in single-crystal copper

Slip system	Burgers vector	Slip plane
1	$[10\bar{1}]$	(111)
2	$[\bar{1}01]$	$(1\bar{1}1)$
3	[011]	$(1\bar{1}1)$
4	[011]	$(11\bar{1})$
5	$[\bar{1}10]$	$(11\bar{1})$
6	[110]	$(\bar{1}11)$
7	$[1\bar{1}0]$	(111)
8	[110]	$(1\bar{1}1)$
9	$[0\bar{1}1]$	(111)
10	$[01\bar{1}]$	$(\bar{1}11)$
11	[101]	$(11\bar{1})$
12	[101]	$(\bar{1}11)$

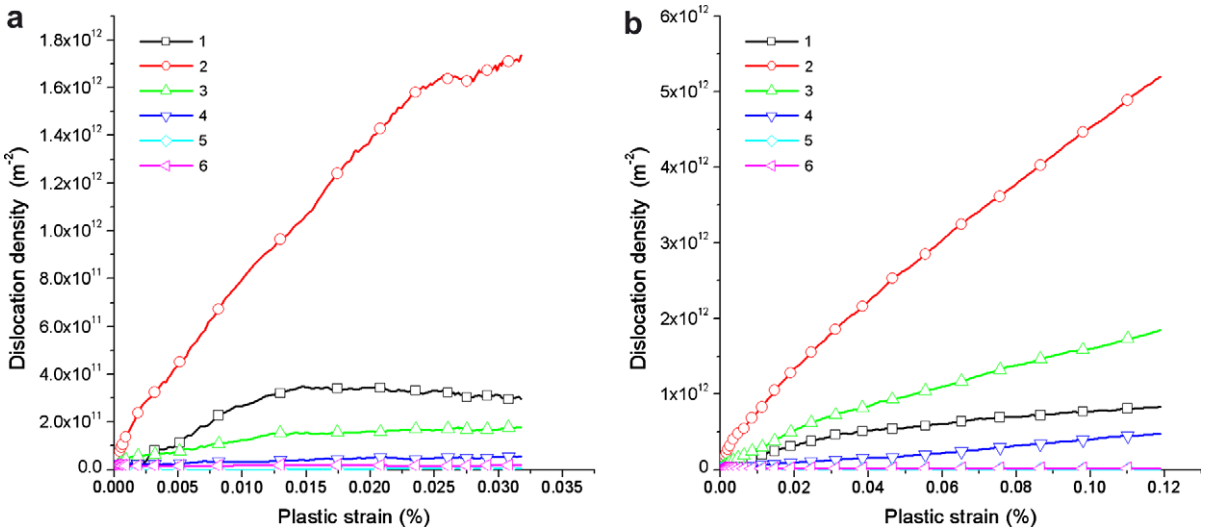

Fig. 9. The dislocation density evolution in different slip systems under strain rate (a) $10^4\ s^{-1}$ (b) $10^5\ s^{-1}$.

dislocation sources of Frank-Read-type are slow-acting, they cannot supply a quantity of dislocations that would suffice for an appreciable plastic strain rate during a small time interval any more, and the new physical mechanisms of dislocation multiplication or generation are still lacking (Bringa et al., 2006; Shehadeh et al., 2006).

The stress distributions in the single-crystal copper under different strain rates are also investigated. Trasca stress distributions are plotted in Fig. 10, which is relatively higher in the band comparing with those in the neighboring regions, and that will induce the materials in the bands to lose the ability to transfer the shear stress, leading to the shear instability of material. As also can be seen from Fig. 10, there are some stress and strain concentration regions in the band because of the heterogeneity of plastic deformation, and they are often the locations where further failure occurs, such as the formation of crack and growth of void (Wright, 2002). Shear band must be given more attention for crystalline material under high-strain-rate deformation.

5. Concluding remarks

The combined dislocation dynamics and FE simulation for the mechanical response of single-crystal copper under different loading rates are performed on the mesoscale.

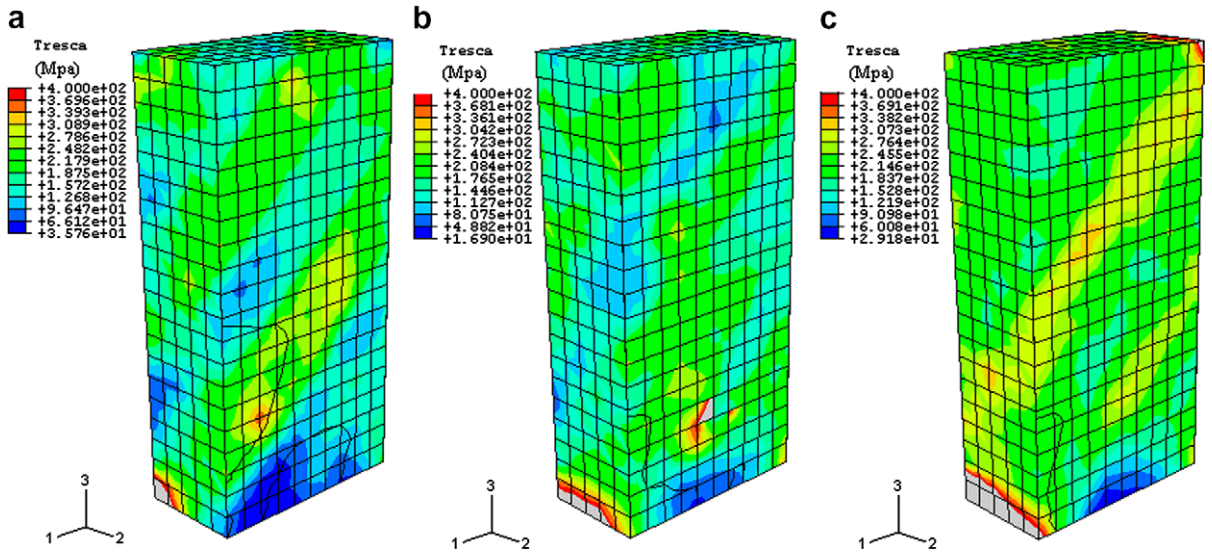

Fig. 10. Distribution of Tresca stress in the crystal after yield under strain rate (a) $10^3\ s^{-1}$, (b) $10^4\ s^{-1}$, (c) $10^5\ s^{-1}$.

With the increasing of strain rate, the yield stress of single-crystal copper increases, and a critical strain rate exists for each single-crystal copper block for given size and dislocation sources, which is determined by the initial dislocation density, the average size of the dislocation mean free path, and the strength of the barriers of dislocation. Below the critical strain rate, the yield stress is relatively insensitive to the strain rate, and above it, the yield stress will increase rapidly with the increasing strain rate. It has a linear relationship with $\log \dot{\varepsilon}$. Under high-strain-rate, the dislocation structure patterning changes from non-uniform to uniform and dislocations are localized in one slip systems. Deformation bands are also observed in the simulations, and the band width increases with the strain rate. Shear stress in the band is higher than that in the neighboring region, which may induce the shear instability of crystalline materials. Some material points in the band will be the location where further failures occur because of stress and strain concentration.

With the increasing strain rate, such as under shock loading, temperature in the material will arise considerably, which will affect the material properties and the dislocation mobility. On the other hand, the plastic deformation mechanism may transform from slip to twinning, etc. These effects will be taken into account in future research.

Acknowledgments

The support of the National Natural Science Foundation of China (NSFC) under Grant No. 10772096 is gratefully acknowledged. The authors are grateful to Dr. Devincre for some discussions about dislocation dynamics code microMegas.

References

Bringa, E.M., Rosolankova, K., Rudd, R.E., Remington, B.A., Wark, J.S., Duchaineau, M., Kalantar, D.H., Hawreliak, J., Belak, J., 2006. Shock deformation of face-centered-cubic metals on subnanosecond timescales. Nat. Mater. 5, 805.

Becker, R., 1925. Elastische nachwirking und plastizitat. Z. Phys. 26, 919.

Bulatov, V.V., 2002. Current developments and trends in dislocation dynamics. J. Computer-aided Mater. Des. 9, 133–144.

Chen, Y.J., Meyers, M.A., Nesterenko, V.F., 1999. Spontaneous and forced shear localization in high-strain-rate deformation of tantalum. Mater. Sci. Eng. A268, 70.

Devincre, B., Kubin, L.P., 1997. The modeling of dislocation dynamics: elastic behavior versus core properties. Phil. Trans. R. Soc. Lond. A 355, 2003–2012.

Devincre, B., Kubin, L.P., 2001. Mesoscopic simulations of plastic deformation. Mater. Sci. Eng. A309-310, 211–219.

Devincre, B., Kubin, L.P., 2006. Physical analyses of crystal plasticity by DD simulations. Scripta Mater. 54, 741–746.

Devincre, B., Condat, M., 1992. Model validation of a 3D simulation of dislocation dynamics: discretization and line tension effects. Acta Metall. Mater. 40, 2629–2637.
Daw, M.S., Baskes, M.I., 1984. Embedded-atom method: derivation and application to impurities, surfaces, and other defects in metals. Phys. Rev. B 29 (12), 6443.
Edington, J.W., 1969. The influence of strain rate on the mechanical properties and dislocation substructure in deformed copper single crystals. Phil. Mag. 19 (162), 41.
Fivel, M., 1998. Mesoscopic scale simulation of dislocation dynamics in fcc metals: principles and applications. Model. Simul. Mater. Sci. Eng. 6, 755–770.
Follansbee, P.S., Gray, G.T., 1991. Dynamic deformation of shock prestrained copper. Mater. Sci. Eng. A 138, 23.
Gillis, P.P., Gilman, J.J., Taylor, J.W., 1969. Stress dependences of dislocation velocities. Phil. Mag. 20, 278.
Gillis, P.P., Kratochvil, J., 1970. Dislocation acceleration. Phil. Mag. 21, 425.
Guo, Y., Zhuang, Z., Li, X.Y., Chen, Z., 2007. An investigation of the combined size and rate effects on the mechanical responses of FCC metals. Int. J. Solids Struct 44, 1180–1195.
Holian, B.L., Lomdahl, P.S., 1998. Plasticity induced by shock waves in nonequilibrium molecular-dynamics simulations. Science 280 (3725), 2085.
Hirth, J.P., Lothe, J., 1982. Theory of Dislocations. Wiley, New York.
Horstemeyer, M.F., Baskes, M.I., Plimpton, S.J., 2001. Length scale and time scale effects on the plastic flow of FCC metals. Acta. Mater. 49, 4363.
Hoagland, R.G., Baskes, M.I., 1998. An atomistic study of the effects of stress and hydrogen on a dislocation lock in nickel. Scripta Mater. 39 (4-5), 417.
Lemarchand, C., Devincre, B., 2001. Homogenization method for a discrete-continuum simulation of dislocation dynamics. J. Mech. Phys. Solids 49, 1969–1982.
Liang, W., Zhou, M., 2004. Response of copper nanowires in dynamic tensile deformation. Proc. Inst. Mech. Eng. Part C: J. Mech. Eng. Sci. 218 (6), 599.
Liu, X.H., Schwarz, K.W., 2005. Modeling of dislocations intersecting a free surface. Model. Simul. Mater. Sci. Eng. 13, 1233–1247.
Meyers, M.A., 1994. Dynamic Behavior of Materials. John Wiley & Sons, New York.
Meyers, M.A., Benson, D.J., Kad, B.K., 2002. Constitutive description of dynamic deformation: physically-based mechanisms. Mater. Sci. Eng. A322, 194–216.
Meyers, M.A., Gregori, F., Kad, B.K., 2003. Laser-induced shock compression of mono-crystalline copper: characterization and analysis. Acta Mater. 51, 1211–1228.
Needleman, A., 1999. Computational mechanics at the mesoscale. Acta Mater. 48, 105–124.
Peirce, D., Asaro, R.J., Needleman, A., 1982. Material rate dependence and localized deformation in crystalline solid. Acta Metall. 31, 1951–1976.
Seeger, A., 1954. Theorie der Kristallplastizitat. Z. Naturforsch. 9A, 758.
Shehadeh, M.A., Bringa, E.M., Zib, H.M., Mcnaney, J.M., Remington, B.A., 2006. Simulation of shock-induced plasticity including homogeneous and heterogeneous dislocation nucleations. Appl. Phys. Lett. 89, 171918.
Tadmor, E.B., Phillips, R., Ortiz, M., 2000. Hierarchical modeling in the mechanics of materials. Int. J. Solids Struct. 37, 379–389.
Taylor, P., Dodson, B.W., 1990. Propagating lattice instabilities in shock-loaded metals. Phys. Rev. B 42 (2), 1200.
Van der Giessent, E., Needleman, A., 1995. Discrete dislocation plasticity: a simple planar model. Mater. Sci. Eng. 3, 689–735.
Wright, T.W., 2002. The Physics and Mathematics of Adiabatic Shear Bands. Cambridge University Press, Cambridge.
Zerilli, F.J., Armstrong, R.W., 1987. Dislocation-mechanics-based constitutive relations for material dynamics calculations. J. Appl. Phys. 61, 1816.
Zerilli, F.J., Armstrong, R.W., 1990. Description of tantalum deformation behavior by dislocation mechanics based constitutive relations. J. Appl. Phys. 68, 915.
Zbib, H.M., Diaz de la Rubia, T., 2002. A multiscale model of plasticity. Int. J. Plast. 18, 1133–1163.
Zhou, F., Wright, T.W., Ramesh, K.T., 2006. A numerical methodology for investigating the formation of adiabatic shear band. J. Appl. Phys. 54, 904–926.